JOURNAL OF THE AMERICAN CHEMICAL SOCIETY

Article

Electrical Discharge in a Nanometer-Sized Air/Water Gap Observed by Atomic Force Microscopy

Xian Ning Xie, Hong Jing Chung, Chorng Haur Sow, Kazimierz Adamiak, and Andrew Thye Shen Wee

J. Am. Chem. Soc., **2005**, 127 (44), 15562-15567• DOI: 10.1021/ja054225r • Publication Date (Web): 04 October 2005

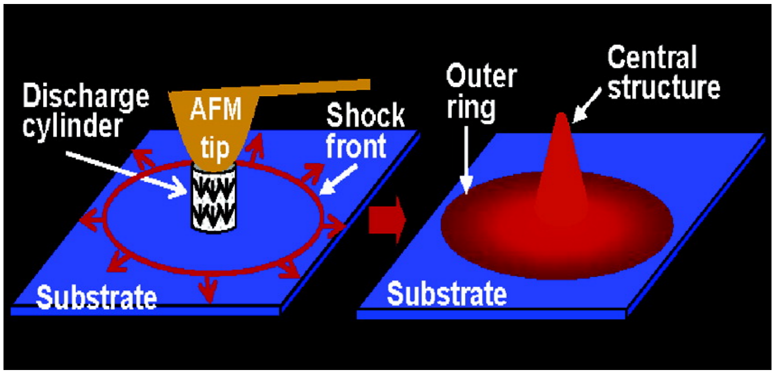

JACS

ARTICLES

Electrical Discharge in a Nanometer-Sized Air/Water Gap Observed by Atomic Force Microscopy

Xian Ning Xie,*,† Hong Jing Chung,†,‡ Chorng Haur Sow,†,‡
Kazimierz Adamiak,*,§ and Andrew Thye Shen Wee*,†,‡

Contribution from the NUS Nanoscience and Nanotechnology Initiative (NUSNNI), and
Department of Physics, National University of Singapore, 2 Science Drive 3, Singapore, 117542,
and Department of Electrical and Computer Engineering, University of Western Ontario,
London, Ontario, Canada N6A 5B9

Received June 27, 2005; E-mail: phyweets@nus.edu.sg (A.T.S.W.); nnixxn@nus.edu.sg (X.N.X.); kadamiak@eng.uwo.ca (K.A.)

Abstract: We report a method to initiate and investigate electrical discharges of ambient air/water molecules in a nanometer-sized gap. Our methodology is based on a typical atomic force microscopy (AFM) setup, in which a cylinder discharge gap of ≤5 nm could be configured between the AFM probe and substrate. We observed highly localized stochastic nanoexplosions in which the discharge probability is dominated by the electric field, material-specific surface reactions, and humidity. AFM results, coupled with the boundary element method (BEM), finite element method (FEM), and method of characteristics (MOC) simulations, further revealed the generation of transient shock waves in the nanoscale discharge. The propagation of shock fronts significantly facilitates the radial expansion of the ionized particles, leading to the formation of microscale patterns on selected substrates. Our findings provide an initial understanding of nanoscale discharge and could be relevant to a few applications including nano/microstructuring, microelectronics, and plasma-assisted depositions.

Introduction

The discharge of gases is usually triggered by ionizations under conditions of high temperature, high electrical field, or strong optical radiation.[1−5] In dry gases, the primary ionization is initiated by seed electrons, and subsequent ionizations are self-sustained by avalanching electron−molecule collisions. The current and charge distribution in the discharge is governed by Laplacian and space charge fields.[1−5] Controlled gas discharges have wide applications in micromachining,[6−8] thin film growth,[9,10] gas-filled switching devices,[11] pollutant removal[12,13] and microsurgery.[14,15] In laser-induced gas breakdown, the energy liberated from the plasma was exploited to modify semiconductors[6−8] and decompose energetic polymers.[16] Yet, our understanding of gas breakdown has been restricted to bulky gas discharges which often spread over large areas.[6−10] The emerging nanotechnology demands functional structures to be defined with nanometer accuracy for miniaturized devices and improved performance.[17−19] For example, memory bits with diameter of ∼40 nm and bit spacing of <100 nm have to be fabricated to achieve a potential storage density of 400 Gbyte/in^2 on polymer.[18,19] Highly localized gas discharges are also desirable for site-specific deposition of single nanostructures in chemical vapor deposition.[10] One possible solution to this challenge is to realize nanoscale control of discharges in lithographical and depositional techniques, which essentially involve the ionization of neutral species. To date, an observation and understanding of nanodischarge has not been gained due to (i) the difficulty in setting up a nanodischarge device and (ii) the lack of suitable tools to monitor the spatial and temporal evolution of the

---

[*] Address general correspondence to A.T.S.W. and X.N.X.; address inquiries pertaining to BEM/FEM/MOC simulations to K.A.

[†] NUS Nanoscience and Nanotechnology Initiative, National University of Singapore.

[‡] Department of Physics, National University of Singapore.

[§] University of Western Ontario

(1) Sigmond, R. S.; Goldman, M. *Electrical Breakdown and Discharges in Gases, Part B Macroscopic Processes and Discharges*; Kunhardt, E. E., Luessen, L. H., Eds.; Plenum Press: New York, 1983; pp 1−64.
(2) Wijsman, R. A. *Phys. Rev.* **1949**, *75*, 833.
(3) Christophorou, L. G. *Electron−Molecule Interactions and Their Application*; Academic: New York, 1984.
(4) Lachaud, S.; Loiseau, J. F. *Eur. Phys. J. Appl. Phys.* **2003**, *24*, 67−74.
(5) Fouad, L.; Elhazek, S. *J. Electrostat.* **1995**, *35*, 21.
(6) Glezer, E. N.; Mazur, E. *Appl. Phys. Lett.* **1997**, *71*, 882.
(7) Georgiev, D. G.; Baird, R. J.; Avrutsky, I.; Auner, G.; Newaz, G. *Appl. Phys. Lett.* **2004**, *84*, 4881.
(8) Dolgaev, S. I.; Lavrishev, S. V.; Lyalin, A. A.; Simakin, A. V.; Voronov, V. V.; Shafeev, G. A. *Appl. Phys. A* **2001**, *73*, 177.
(9) Mazouffre, S.; Vankan, P.; Engeln, R.; Schram, D. C. *Phys. Rev. E: Stat. Phys., Plasmas, Fluids, Relat. Interdiscip. Top.* **2001**, *64*, 066405.
(10) Schram, D. C. *Pure Appl. Chem.* **2002**, *74*, 369.
(11) Kristiansen, M.; Guenther, A. H. *Electrical Breakdown and Discharges in Gases, Part B Macroscopic Processes and Discharges*; Kunhardt, E. E., Luessen, L. H., Eds.; Plenum Press: New York, 1983; pp 383−414.
(12) Lee, J. M.; Watkins, K. G. *J. Appl. Phys.* **2001**, *89*, 6496.
(13) van Veldhuizen, E. M. *Electrical Discharges for Environmental Purposes: Fundamentals and Applications*; Nova Science Publishers Inc., 2000; p 432.
(14) Venugopalan, V.; Guerra, A., III; Nahen, K.; Vogel, A. *Phys. Rev. Lett.* **2002**, *88*, 078103.
(15) Haupt, G. *J. Urol.* **1997**, *158*, 4.
(16) Ben-Eliahu, Y.; Haas, Y.; Welner, S. *J. Phys. Chem.* **1995**, *99*, 6010.
(17) Xia, Y.; Rogers, J. A.; Paul, K. E.; Whiteside, G. M. *Chem. Rev.* **1999**, *99*, 1823.
(18) Vettiger, P.; Cross, G.; Despont, M.; Drechsler, U.; Dürig, U.; Gotsmann, B.; Häberle, W.; Lantz, M. A.; Rothuizen, H. E.; Stutz, R.; Binnig, G. K. *IEEE Trans. Nanotechnol.* **2002**, *1*, 39.
(19) Lutwyche, M. I.; Despont, M.; Drechsler, U.; Durig, U.; Haberle, W.; Rothuizen, H.; Stutz, R.; Widmer, R.; Binnig, G. K.; Vettiger, P. *Appl. Phys. Lett.* **2000**, *77*, 3299.

10.1021/ja054225r CCC: $30.25

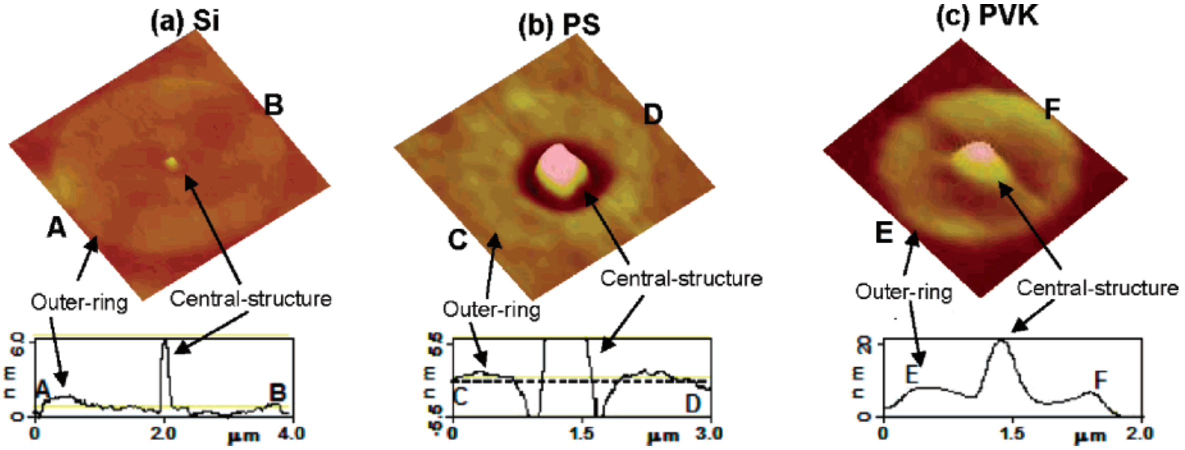

Figure 1. AFM height images showing the central and outer structures produced on (a) Si with 18 V bias and 2 s duration, (b) PS with 35 V bias and 2 s duration, and (c) PVK with 10 V bias and 2 s duration, respectively.

nanoscale discharge.[13,20] Atomic force microscopy (AFM) proves to be an excellent technique for in situ nanolithography and characterization.[21−24] In this work, we demonstrate the use of a typical AFM setup to configure a nanoexplosion device and image the spatial distribution of the discharge. In our method, the stationary AFM probe was engaged with a flat substrate, such that a discharge cylinder with a basal radius of 20−50 nm (typical tip radius of curvature) and height of ≤5 nm[23,25] (typical tip−substrate spacing) was formed. A negative voltage was applied to the conductive tip to initiate the discharge in an ambient air/water gap. Suitable substrates were selected to ensure that the ionized molecules could react with the substrates to produce specific patterns from which one can deduce the spatial distribution of the ionized particles. We discovered highly localized discharges which led to the formation of central nanostructures on the substrates. Moreover, transient shock waves were also observed to expand the trajectory of reactive ions and form microscale outer rings surrounding the central structures. The stochastic nature of the nanoexplosion was further illustrated in terms of its occurrence probability on different substrates and under various humidity conditions.

Experimental Section

Polystyrene (PS, M_w = 1100 k) and poly(*N*-vinyl carbazole) (PVK, M_w = 1100 k) were both purchased from Aldrich and used without further purification. Si (100) substrates were sonicated in ethanol, rinsed with acetone, and blow-dried in N_2 gas. The PS films were prepared by spin-coating from 5 wt % solution in dichloroethane onto Si substrates followed by drying under a N_2 atmosphere. A solution of 0.5 wt % PVK in toluene was also spin-coated onto Si substrates. The PVK films were then annealed in a vacuum oven for 2 h at 175 °C. The thickness of the PS and PVK films are ~90 and ~70 nm, respectively, as determined by atomic force microscopy (AFM). A NanoMan AFM system (Nanoscope IV, Veeco Inc.) was operated in air for all the AFM-based discharges and measurements (see Supporting Information S1 for details). The numerical algorithm for the nanodischarge was based on three techniques: BEM (boundary element method), FEM (finite element method), and MOC (method of characteristics). BEM was used to obtain the solution of the Laplacian electric field where the space charge was assumed to be zero and only the applied static voltage was considered. BEM solution was then applied to generate FEM mesh (see Supporting Information S2 for details).

Results and Discussion

Figure 1 shows the AFM height images of structures created after tip bias application on Si, polystyrene (PS), and poly(N-vinyl carbazole) (PVK) materials, respectively. The patterns are characterized by a central structure surrounded by an outer ring. The width of the central structure is between 90 and 600 nm, and the diameter of the outer ring ranges from 0.4 to 5.0 μm. In the case of Si, (see Figure 1a), the raised central dot and outer ring are oxide products of the probed-assisted anodic oxidation.[21,23] On PS (see Figure 1b), the structure formation is due to tip-induced polymer melting and mass transport as previously observed in various polymeric materials.[25−30] As for PVK (see Figure 1c), the formation of the central cone and outer ring arises from PVK cross-linking and oxygenation under high electrical field.[31] These structures are not attributable to deposited surface charges, as they are different in shape, and were produced on both semiconducting Si and insulating PS and PVK substrates. Furthermore, both the central and outer oxides on Si could be preferentially etched by dilute hydrofluoric (HF) acid, confirming the chemical identity of the oxide patterns. The typical field applied in the tip−substrate gap reached 10^7−10^{10} V/m, which is higher than the breakdown field of

---

(20) Li, Y. T.; Zhang, J.; Sheng, Z. M.; Teng, H.; Liang, T. J.; Peng, X. Y.; Lu, X.; Li, Y. J.; Tang, X. W. *Phys. Rev. Lett.* **2003**, *90*, 165002.

(21) Snow, E. S.; Jernigan, G. G.; Campbell, P. M. *Appl. Phys. Lett.* **2000**, *76*, 1782.

(22) Lee, K.-B.; Park, S.-J.; Mirkin, C. A.; Smith, J. C.; Mrksich, M. *Science* **2002**, *295*, 1702.

(23) Xie, X. N.; Chung, H. J.; Xu, H.; Xu, X.; Sow, C. H.; Wee, A. T. S. *J. Am. Chem. Soc.* **2004**, *126*, 7665.

(24) Gómez-Moñivas, S.; Sáenz, J. J.; Calleja, M.; García, R. *Phys. Rev. Lett.* **2003**, *91*, 056101.

(25) Lyuksyutov, S. F.; Vaia, R.; Paramonov, P. B.; Juhl, S.; Waterhouse, L.; Ralich, R. M.; Sigalov, G.; Sancaktar, E. *Nat. Mater.* **2003**, *2*, 468.

(26) Juhl, Sh.; Phillips, D.; Vaia, R. A.; Lyuksyutov, S. F.; Paramonov, P. B. *Appl. Phys. Lett.* **2004**, *85*, 3836.

(27) Lyuksyutov, S. F.; Paramonov, P. B.; Sharipov, R. A.; Sigalov, G. *Phys. Rev. B: Condens. Matter* **2004**, *70*, 174110.

(28) Lyuksyutov, S. F.; Paramonov, P. B.; Juhl, Sh.; Vaia, R. A. *Appl. Phys. Lett.* **2003**, *83*, 4405.

(29) Schaffer, E.; Thurn-Albrecht, T.; Russell, T. P.; Steiner, U. *Nature* **2000**, *403*, 874.

(30) Xie, X. N.; Chung, H. J.; Sow, C. H.; Bettiol, A. A.; Wee, A. T. S. *Adv. Mater.* **2005**, *17*, 1386.

(31) The structure and composition of patterns formed on PVK were examined using conducting atomic force microscopy, photoemission spectroscopy, Fourier infrared spectroscopy, and density functional theory calculations. It was found that the structure formation is due to the cross-linking of carbazole groups in PVK by bridge oxygen. These results will be published elsewhere.

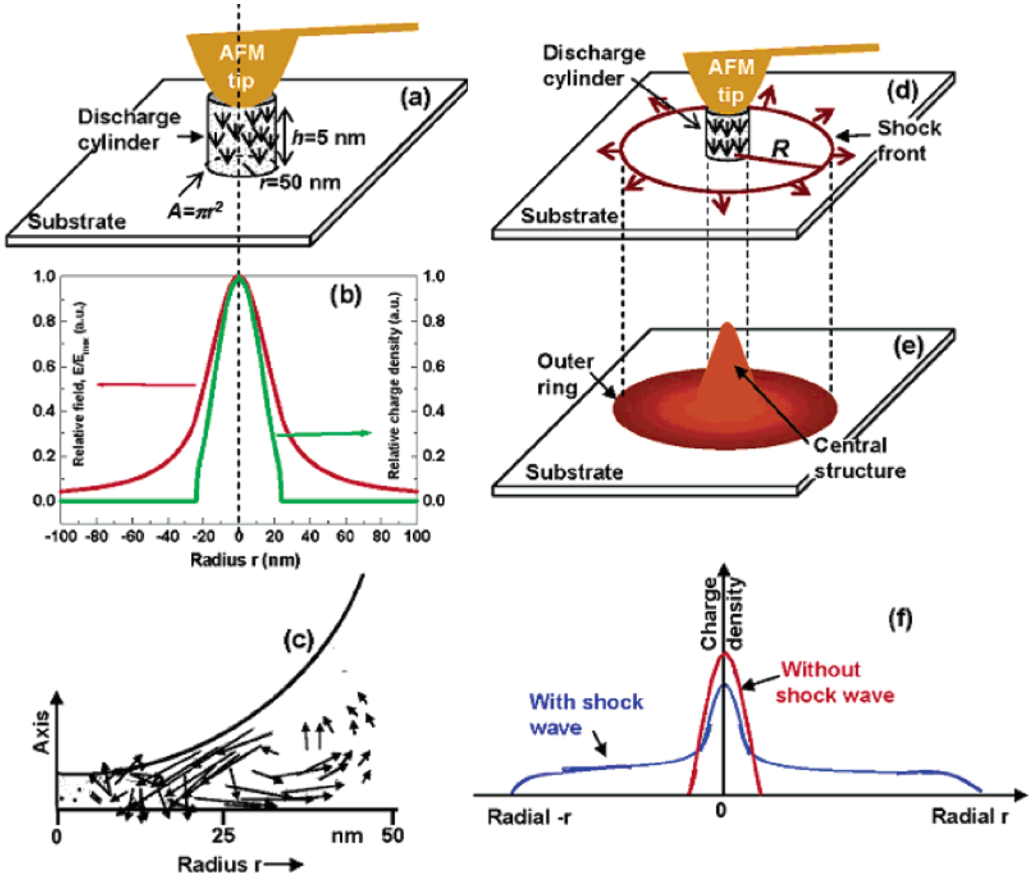

Figure 2. Left column: hybrid BEM/FEM/MOC simulation of field/charge distribution and ionic wind in the nanometer-sized discharge gap. (a) Geometry of the discharge device consisting of the AFM tip (cathode), substrate (anode), and the discharge cylinder with a height of $h = 5$ nm and basal area of $A = \pi r^2$ where $r = 50$ nm. (b) Calculated field/charge density radial distributions in the local discharge gap. (c) Calculated velocity vectors of the airflow in the discharge gap. Right column: proposed shock wave generation and lateral expansion of charge density by the shock front. (d) Propagation of shock waves induced by the nanoexplosion. (e) Outer ring formation by the shock wave assisted charge density expansion. (f) Comparison of charge density radial distribution between explosions with and without shock wave formation.

humid air of ~3 × 10^6 V/m.[32] The high field, along with the large ionic current observed during pattern formation (to be discussed in Figure 3d), suggests the initiation of discharge/breakdown of the air/water dielectric. A hybrid BEM (boundary element method), FEM (finite element method), and MOC (method of characteristics) simulation[33] was carried out to examine the field and charge distributions in the discharge cylinder shown in Figure 2a. The height h and basal radius r of the discharge cylinder were assumed to be 5 and 50 nm, respectively, which are based on the typical tip−substrate spacing and tip radius of curvature used in AFM experiments. The computational algorithm consists of two iterative loops, the inner loop for electric field and space charge density, and the outer loop for charge density on the probe surface (see Supporting Information S2). It can be seen in Figure 2b that both the field and charge density are highly confined to the vicinity of the tip apex even in the event of air/water discharge. The field is the maximum ($E_{\max}$) at the axial position ($r = 0$). It decays by ~80% at a radial distance of $r = 40$ nm, and it is only 5% of $E_{\max}$ at $r = 100$ nm. The charge density, which decreases more steeply, is extremely localized inside a circle of $r \leq 25$ nm. There is essentially no charge distribution outside the circular area as shown in Figure 2b. The above results were calculated for a conductive metal substrate by assuming an equipotential on the surface. For the semiconducting and insulating samples used in our experiments, there will be charge accumulation on the substrates, and we were unable to simulate this effect due to the constraint of our computing code. Nevertheless, previous works[34−39] have indicated that charge deposition would mainly reduce the magnitude of the electric field in the tip−surface gap, while having no significant impact on the radial extent of the field (see discussion in the next paragraph). Similar charge densities have been calculated for charged and uncharged dielectric layers in ref 34. When the lateral dimension of the structures in Figure 1 are compared with the radial distribution of field and charge density in Figure 2b, it is evident that the local discharge provides good account for the central structure formation. That is, the strong field and high charge concentration in the axial position promote the oxidation on Si, mass transport on PS, and cross-linking/oxygenation on PVK, respectively. However, the localized discharge cannot explain the formation of outer rings which

---

(32) van Veldhuizen, E. M.; Ruters, W. R. *J. Phys. D: Appl. Phys.* **2003**, *36*, 2692.
(33) Zhao, L.; Adamiak, K. *J. Electrostat.* **2005**, *63*, 337.
(34) Abdel-Salam, M.; Singer, H.; Ahmed, A. *J. Phys. D: Appl. Phys.* **2001**, *34*, 1219.
(35) Blennow, H. J. M.; Sjöberg, M. L.-Å.; Leijon, M. Å. S.; Gubanski, S. M. *IEEE Trans. Dielectr. Electr. Insul.* **2000**, *7*, 340.
(36) Sjöberg, M.; Serdyuk, Yu. V.; Gubanski, S. M.; Leijon, M. Å. S. *J. Electrostat.* **2003**, *59*, 87.
(37) Pépin, M. P.; Wintle, H. J. *J. Appl. Phys.* **1998**, *83*, 5870.
(38) Lachish, U.; Steinberger, I. T. *J. Phys. D: Appl. Phys.* **1974**, *7*, 58.
(39) Atkinson, P. J.; Fleming, R. J. *J. Phys. D: Appl. Phys.* **1980**, *13*, 625.

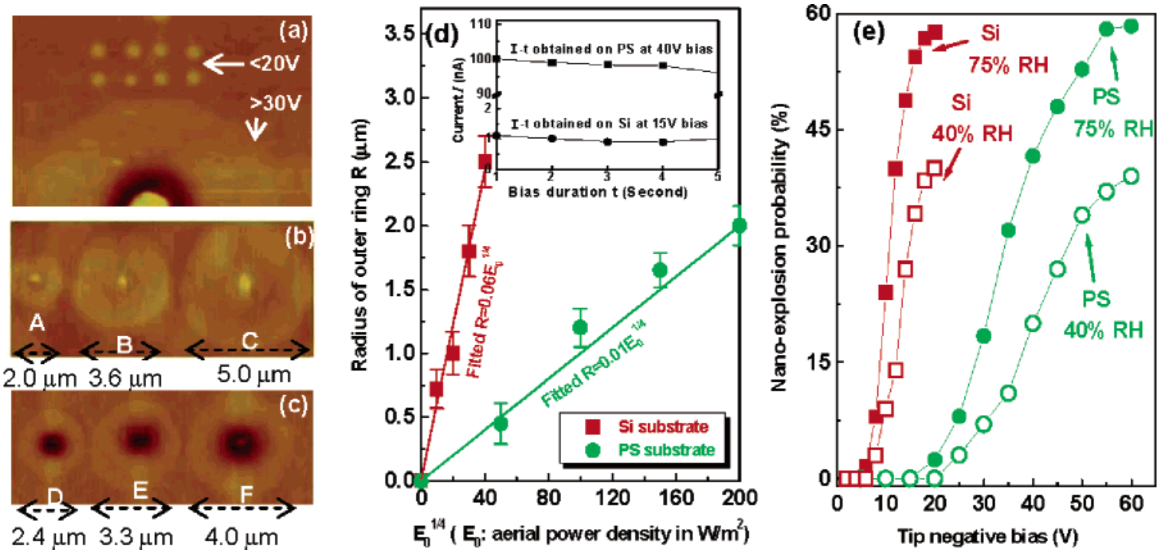

Figure 3. (a) AFM image showing tiny dot formation by partial ionization (bias <20 V) and large outer ring formation by strong nanoexplosion and shock wave propagation (bias ≥ 30 V) on PS. (b) AFM image of oxide structures A, B, and C produced on Si with 12, 15, 18 V bias voltage and 5 s bias duration, respectively. (c) AFM images of structures D, E, and F created on PS with 30, 40, and 50 V bias voltage and 5 s bias durations, respectively. Pits are formed in the center due to polymer ablation by prolonged bias duration. (d) Fitted $R \sim E_0^{1/4}$ linearity, where R (in micrometers) is the radius of the outer rings and E_0 (in W/m^2) is the nominal aerial power density released from the nanoexplosion. The inset shows the temporal evolution of current ($I-t$ curves) recorded during discharge. (e) Nanoexplosion probability as a function of tip voltage obtained statistically on Si and PS under relative humidities (RH) of 75% and 40%, respectively.

are up to 100 times the radial dimension of charge density. The contribution of ionic wind to expanding charge density is negligible, as the air in the gap can only flow to a maximum radial distance of 80 nm (see Figure 2c). The calculated radial velocity of the air flow is almost zero at radial distances of $r >$ 50 nm (see Supporting Information S2, Figure S1). Therefore, we suggest that the local discharge is essentially a nanoexplosion, which can generate transient shock waves when a large amount of discharge energy is released rapidly onto a small volume. Indeed, shock waves triggered by large scale electric discharge[40] and laser-induced breakdown[16] have been reported before. As illustrated in Figure 2d−f, the propagation of the shock front can significantly expand the charge density out of the cylindrical zone to facilitate the formation of microscale outer rings.

It is instructive to elaborate more on the mechanism for the formation of the outer ring shown in Figure 1. Previously, Lyuksyutov et al observed similar oxide structures formed on Si under high AFM probe bias.[41] The authors ascribed the formation of such structures to the creation and breakdown of the ion-hole space charge double layer at the water-Si interface. In the event of double-layer breakdown, the variation in the field-induced hole concentration results in regions of depleted holes affecting the formation of the space charge layer. The hydroxyl ion distribution follows the profile of the hole concentration, and oxide is formed in areas of maximum hole concentration. The authors also observed anomalously high electrical current (up to 500 μA) accompanying the breakdown process.[41] Here in our experiments, OH^-, O^-, and O^{2-} ions are deposited onto the substrates such as Si due to the ambient air discharge. The negative ions would induce an electrically inverted layer of holes in the subsurface region of Si, thus forming the so-called space charge double layer.[41] The lateral dimension of the double layer should follow the radial distribution of the electric field, as the density distribution of the negative ions (which induced the double layer) is predominantly determined by the electric field. It has been shown that for charge accumulation on dielectrics, the surface charge density would be sharply peaked (usually in a bell shape) in the region close to the injecting electrode.[37−39] At room temperature, the spreading of surface charge by thermal diffusion can be discounted, as the equivalent thermal voltage is negligibly low ($kT/q \approx 0.025$ V) compared to the electrical voltage.[37,42] Therefore, the radial dimension of the surface charge or double layer would usually be limited by the surface coverage of the electric field and ionic trajectory. The double-layer breakdown was not evident in our experiments, as the ionic current detected in the patterning of Si is quite stable and is in the region of ∼1 nA at a tip bias of 15 V (see Figure 3d). Based on the simulated results shown in Figure 2, we suggest that the double layer is also localized in the vicinity of the tip apex, and the negative ions on the top layer react with Si to produce the central oxide structure. The outer ring formation can be attributed to the expansion of the ion trajectories by shock wave propagation. The expanded ions could deposit on surface sites 0.5−2.5 μm away from the center, where a similar double layer is induced, and ring-shaped oxides are subsequently formed as a result of anodic oxidation.

We now further address the role of shock front propagation in expanding the local discharge. In Figure 3a, eight tiny dots (∼150 nm wide, ∼6 nm high) were produced on PS at low voltages (<20 V) without the initiation of a nanoexplosion. The contrast between the nanodots and the nearby microscale ring produced with the initiation of nanoexplosion at high voltages (≥ 30 V) signifies the strong impact of gas discharge and shock wave generation on the pattern formation. As seen in Figure 3, parts b and c, the diameter of the outer rings grows with

---

(40) Voitenko, A. E.; Model, I. S. *Sov. Phys. JEPT* **1963**, *17*, 1180.
(41) Lyuksyutov, S. F.; Paramonov, P. B.; Dolog, I.; Ralich, R. M. *Nanotechnology* **2003**, *14*, 716.
(42) Mott, N. F.; Gurney, R. W. *Electric Processes in Ionic Crystals*, 2nd ed.; Oxford University Press: London, 1948; p 172.

increasing tip voltage on both Si and PS. For a strong shock,[16,43] the mass of air encompassed by the shock wave's radius (proportional to πR^2 in Figure 2d) is much larger than that of the initial air at the explosion site (proportional to πr^2 in Figure 2d). The nominal aerial power density E_0 liberated from the nanoexplosion was estimated using the relation $E_0 = UI/\pi r^2$, where U is the tip voltage and I the electrical current recorded simultaneously during bias application. The effective power density E_{eff} responsible for shock wave generation is proportional to the nominal power density E_0 via $E_{\text{eff}} = \beta E_0$, where β is a system-specific scaling factor. The radius of the shock front R at time t can be further obtained by solving the state equations using similarity and dimensional methods[43]

$$R = \theta(E_{\text{eff}}/\rho_0)^{1/4}t^{1/2} = fE_0^{\ 1/4} \qquad (1)$$

where ρ_0 is the density of air, θ is a constant related to the heat capacity of air, and f is a simplified fitting parameter which absorbs ρ_0, θ, t, and β. Under the same ambient conditions and bias duration t, R is proportional to $E_0^{\ 1/4}$. A quantitative fit of experimental $R \sim E_0$ relation to eq 1 is displayed in Figure 3d. It is seen that the experimental results conform well to the strong shock theory, and a best-fit linearity of $R = 0.06E_0^{\ 1/4}$ and $R = 0.01E_0^{\ 1/4}$ was obtained for Si and PS substrates, respectively. The f parameter fitted for Si substrate is 6 times that for PS film, and this indicates the lower discharge voltage and higher scaling factor β for the Si electrode. The temporal evolution of electric current during bias application is also shown in the inset of Figure 3d, from which the nominal energy density E_0 was derived.

The occurrence of the stochastic nanoexplosion was statistically counted in repeated experiments for Si and PS substrates, and the results obtained under 75% and 40% relative humidity (RH) are shown in Figure 3e. On Si substrate at 75% RH, the explosion was triggered at an onset voltage of 8 V with a probability of ~8%. The probability then grows rapidly with cathode voltage and approaches ~60% for a bias of 20 V, above which destructive structures due to oxide breakdown intervened. For PS substrate at 75% RH, the onset voltage was observed to be 20 V with a probability of 2.3%. The explosion occurrence reached ~60% when the tip voltage was raised to 60 V. Beyond 60 V, serious polymer ablation interfered with the formation of the outer structures. The different onset voltage observed on Si and PS signifies the strong impact of substrate-specific surface reactions on discharge probabilities of identical ambient air in the same gap. It manifests the increased dependence of discharge on anode materials when the discharge gap is reduced to a few nanometers. For such a nanogap, the discharge behavior deviates significantly from the traditional Paschen law valid for large scale discharges.[1] The growth of discharge probability with bias voltage observed in Figure 3e is related to the enhancement of ionization by higher field in the Townsend electron avalanche process.[1−5] A higher field would significantly increase the primary and secondary ionization coefficients α and γ, and larger α and γ values favor a higher discharge probability W according to the relation of $W = 1 - \{\gamma \exp[(\alpha d) - 1]\}^{-1}$, where d is the separation between cathode and anode.[2] It is further seen in Figure 3e that humidity conditions strongly affect the discharge probability. For both Si and PS, the probability decreased by ~33% when the RH was reduced from 75% to 40%. The impact of water on the discharge occurrence is 3-fold: (i) O_2 is a strong electronegative molecule which lowers the secondary ionization coefficient γ through the electron attachment reaction of $O_2 + e = O^- + O$;[3,4] partial replacement of O_2 by the less electronegative H_2O molecule would reduce the degree of electron attachment; (ii) the incorporation of H_2O can reduce the size of the ionization zone, thus facilitating the secondary avalanche in the air/water gap;[5] (iii) it has been proven by Lyuksyutov and co-workers that water ionic dissociation can generate substantial electron flux in the tip−surface junction.[41] On one hand, these electrons could act as seed electrons to initiate the primary ionization in ambient air. On the other hand, the electrons may also speed up the generation of ionic carriers through electron−molecule collision. Under higher humidity conditions, more water is condensed in the vicinity of the AFM tip, and this helps promote the discharge probability of the dielectric medium in the tip−surface gap.

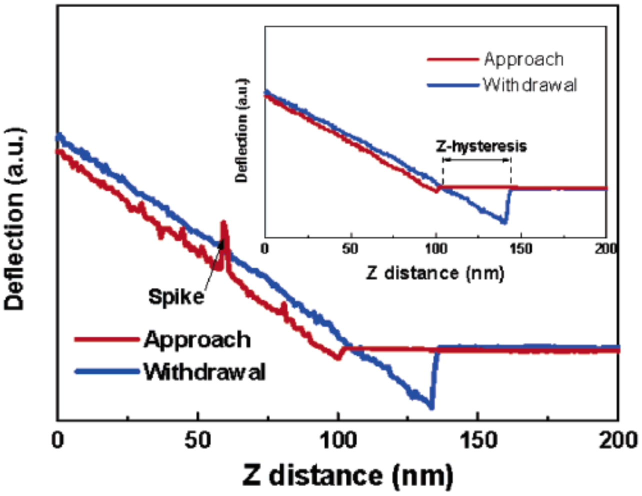

Figure 4. Typical force−distance curves recorded for ramps in which a nanoexplosion was initiated. The inset shows the curves obtained for cycles without the initiation of a nanoexplosion. The two sets of curves were collected under identical conditions with a tip negative bias of 18 V.

The outer and central structures could also be produced on Si by cycling the distance between the biased AFM tip and surface. Specifically, the tip was approached to and withdrawn from the surface using the AFM force−distance measurement function. Under certain tip bias, oxide outer rings were created only in some of the cycles due to the stochastic nature of the nanoexplosion. Figure 4 displays a typical force−distance curve recorded for cycles in which a nanoexplosion was initiated. The force−distance characteristic acquired for those cycles without the initiation of a nanoexplosion was shown in the inset of Figure 4. It can be seen that for cycles without a nanoexplosion, both the approach and withdrawal curves are quite smooth and linear in the repulsive force regime in which the tip is in contact with the surface. A hysteresis between the approach and withdrawal curves (Z-hysteresis) is observed, and it is related to water-induced capillary forces exerted on the tip when it snaps off contact with the surface.[41,44] On the approach curve recorded for cycles with nanoexplosion initiation, small bumps and a sharp spike are observed in the linear repulsive force regime

---

(43) Sedov, L. I. *Similarity and Dimensional Methods in Mechanics*, 10th ed.; CRC Press Inc., 1993; Chapter 4, pp 261−270.

(44) Bloess, H.; Staikov, G.; Schultze, J. W. *Electrochim. Acta* **2001**, *47*, 335.

(see Figure 4). The position and height of the spike might change in different cycles, but it was usually found to be located on the approach curves. The upward spike corresponds to a sudden increase in the repulsive force between the tip and surface. Since it was observed only in the cycles which triggered a nanoexplosion, we suggest that the spike should be induced by the explosive discharge of the ambient air. The sudden release of energy in the tip−surface nanogap could generate instantaneous pushing force against the AFM tip. The pushing force adds to the normal repulsive force exerted on the engaged tip and produces a spike in the force−distance curve shown in Figure 4. It should be noted that the spike only reflects the instantaneous increase of force in the vertical direction. The discharge would generate much higher explosive forces in the lateral direction, as shock waves are predominantly induced along the sample surface for the cylindrical discharge geometry considered in Figure 2. On a final note, it might be informative to perform an oscillographic study of the electrical current for discharges in the nanoscale air/water gap (due to the limit of our experimental setup, we were unable to do so). Discrete Trichel pulsation[45] arising from space charge accumulation and clearing has been observed for large scale discharges in air. Further understanding on the explosive discharge could possibly be attained by probing such pulsation behaviors in the nanoexplosion.

In summary, we have demonstrated a novel approach to investigating and controlling nanoscale discharges in ambient air. Lithographically induced nanoscale discharge and microscale shock wave propagation were observed in the nanometer-sized air/water gap. The explosion and shock waves manifest themselves as central and outer structures on selected substrates. The nanoexplosion occurs stochastically with the probability dominated by the interplay of electric field, relative humidity, and surface reactions. The shock wave propagation, which is associated with the aerial discharge power density, assists to laterally expand the local plasma. An understanding and control of nanoexplosions could open new routes to site-specific nanopatterning and material depositions.

Acknowledgment. We thank Dr. H. Xu and Mr. C. Y. Zhang for valuable discussions. Dr. S. Swaminathan, Mr. J. Subbiah, and Mr. Y. W. Zhu are acknowledged for their help in the AFM experiments. This work is supported by the NUS Nanoscience and Nanotechnology Initiative (NUSNNI), National University of Singapore.

Supporting Information Available: S1 experimental and S2 simulation of nanoscale discharge. This material is available free of charge via the Internet at http://pubs.acs.org.

JA054225R

---

(45) Trichel, G. W. *Phys. Rev.* **1938**, *54*, 1078.